

Interaction induced Dirac fermions from quadratic band touching in models of bilayer graphene

Sumiran Pujari,¹ Thomas C. Lang,² Ganpathy Murthy,¹ and Ribhu K. Kaul¹

¹*Department of Physics & Astronomy, University of Kentucky, Lexington, KY-40506-0055*

²*Institute for Theoretical Physics, University of Innsbruck, 6020 Innsbruck, Austria*

We revisit the effect of local interactions on the quadratic band touching (QBT) of Bernal stacked bilayer graphene models using renormalization group (RG) arguments and quantum Monte Carlo simulations of the Hubbard model. We present an RG argument which predicts, contrary to previous studies, that weak interactions do not flow to strong coupling even if the free dispersion has a QBT. Instead they generate a linear term in the dispersion, which causes the interactions to flow back to weak coupling. Consistent with this RG scenario, in unbiased quantum Monte Carlo simulations of the Hubbard model we find compelling evidence that antiferromagnetism turns on at a finite U/t , despite the $U = 0$ hopping problem having a QBT. The onset of antiferromagnetism takes place at a continuous transition which is consistent with a dynamical critical exponent $z = 1$ as expected for 2+1 d Gross-Neveu criticality. We conclude that generically in models of bilayer graphene, even if the free dispersion has a QBT, small local interactions generate a Dirac phase with no symmetry breaking and that there is a finite-coupling transition out of this phase to a symmetry-broken state.

The interplay of band topology and interactions has taken center stage in condensed matter physics. The interest in band topology was rekindled by the discovery of graphene, where two bands touch at linearly dispersing Dirac points [1]. Short range interactions are well known to be irrelevant at the Dirac fixed point, making the linear band touching a stable many-body phenomenon for weak interactions. Strong interactions trigger an instability to a broken symmetry state [2–4].

Subsequently it was pointed out that bilayer graphene harbors a quadratic band touching (QBT) at half-filling in the nearest neighbor hopping model [5]. Renormalization group studies have shown that interactions are marginally relevant at a QBT [6]. This led to predictions of the stabilization of a symmetry broken state even for arbitrarily weak short-range interactions in bilayer graphene [7, 8] in contrast to single layer graphene. The nature of symmetry broken state depends on the form of the interactions and a plethora of phases have been proposed (see e.g. [7–11]). The Bernal bilayer honeycomb lattice with Hubbard interactions was studied as an example of this kind of ordering [12]. Numerical studies using quantum Monte Carlo concluded that this model was Néel ordered for all values of the coupling U/t consistent with the predictions of weak-coupling [8] and functional renormalization group (RG) [12].

It is well known that on inclusion of certain symmetry preserving hoppings beyond the shortest range (referred to as trigonal warping), a linear term in the dispersion is present at low energies and the QBT splits into four Dirac cones [5]. It has been generally assumed that if the trigonal warping terms are very weak microscopically, for practical purposes they can be neglected – they only cause the symmetry breaking instability to appear at a small interaction strength controlled by their size [13], leading to the RG flow in Fig. 1(a). Here we present arguments and evidence that neglecting linear terms in

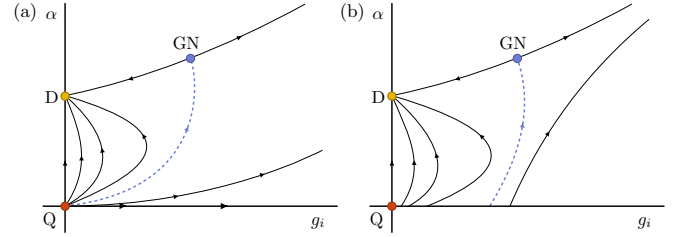


FIG. 1. Two schematics for the renormalization group flows for the Bernal stacked bilayer in the space of α (linear term in the dispersion) and g_i (quartic interactions). [c.f. Eq. (1) for definitions]. The fixed points are Q: quadratic band touching. D: Dirac linear dispersion. GN: Gross-Neveu. (a) The RG flow implied by previous studies. In this scenario, weak interactions always flow to strong coupling when one begins with a QBT, i.e. along $\alpha = 0$. (b) RG flow advocated for in this work, when α arises in an RG flow due to interactions. Note that crucially in (b), α is generated even when one begins on the $\alpha = 0$ line. The point marked as D indicates one of a set of fixed points with $\alpha \neq 0$ which all have a linear Dirac dispersion at low energy, but different details of the electronic structure.

the dispersion is not justified in determining the fate of short range interactions at the quadratic band touching in bilayer graphene. Even in a model Bernal honeycomb bilayer system where the trigonal warping terms are microscopically zero and there is a true QBT in the free problem, interactions will generate the linear term in an RG flow. At weak coupling, we thus conclude that interactions cause the emergence of a Dirac phase from a QBT in bilayer graphene. The instability to a symmetry broken ordered state thus takes place at an order one finite-strength of electron-electron interactions. [c.f. Fig. 1(b)]. Field theoretic arguments suggest that this transition, if continuous, would be of the Gross-Neveu (GN) type [2]. As a concrete test of our RG scenario we present QMC simulations of the Hubbard interaction on

the bilayer graphene lattice. We show that despite the model having a QBT at $U = 0$, interactions cause Néel ordering only at a finite value of $U_c \approx 2.6$. The phase transition between the non-Néel and Néel phase appears to both be continuous and have a dynamical critical exponent $z \approx 1$ consistent with the GN universality class, which further bolsters our identification of Dirac fermions in the weak coupling phase.

RG argument: In the absence of spin-orbit coupling, symmetries guarantee that two spin degenerate low energy bands touch at the \mathbf{K} and \mathbf{K}' points. Expanding around the \mathbf{K} point, a symmetry based study [5, 8] of allowed dispersions for the part quadratic in the fermionic operators Ψ of the Hamiltonian density has the following form up to second order in \mathbf{k} ,

$$H^{(2)} = \Psi_{\mathbf{K}+\mathbf{k}}^\dagger (\text{Re}[\phi(\mathbf{k})]\sigma^x + \text{Im}[\phi(\mathbf{k})]\sigma^y) \Psi_{\mathbf{K}+\mathbf{k}},$$

$$\phi(\mathbf{k}) \equiv \alpha(k_x + ik_y) + \beta(k_x - ik_y)^2 + \mathcal{O}(k^3). \quad (1)$$

The crucial point for our study is that generically a linear term α is allowed by symmetries. At quartic order, $H^{(4)}$ has nine independent symmetry allowed terms of the form $\Psi^\dagger \Psi^\dagger \Psi \Psi$ with coupling constants g_i ($i \in [1, 9]$) [8].

From the RG point of view the quadratic band touching is a fixed point, called Q ($\alpha, g_i = 0$), which has $z = 2$. Power counting shows α is relevant at Q and the g_i are marginal – all other couplings are irrelevant [14]. A one-loop calculation finds that g_i are generically marginally relevant [7, 8]; Q is hence a multicritical point in the RG sense. We now ask how Q is affected when we add only g_i but no α (this corresponds to adding interactions to

a free dispersion with a true QBT). Wilsonian RG tells us that all terms that are allowed by symmetries will appear as we integrate high energy degrees of freedom. Since no symmetry forces $\alpha = 0$ in the dispersion for the Bernal stacked bilayer, it must be generated. Since at Q the linear term is relevant and the interactions are only marginal, at weak coupling the linear term will always grow faster and hence the RG flows will take us to a fixed point with Dirac fermions (see SM for more details). At this fixed point (just like in single layer graphene) interactions are irrelevant. This fixed point, called D, hence has all directions irrelevant and is a stable phase of matter. Once the g_i cross a finite order-one strength they will eventually win over the generated α and a flow to strong coupling will ensue. The separatrix between the flow to weak and strong coupling can flow to an intermediate coupling fixed point, the GN universality class. This RG flow is illustrated in Fig. 1(b). A first order transition, although unlikely given the well established GN scenario, also remains possible in a microscopic model.

Hubbard Model: To provide a concrete lattice realization of the RG argument made above, we present numerical simulations of the Hubbard model on the Bernal stacked honeycomb bilayer. Defining the electron creation operator on sublattice A(B), site i , spin σ and layer ℓ as $a_{i\sigma\ell}^\dagger (b_{i\sigma\ell}^\dagger)$, the Hamiltonian takes the form [15],

$$H_{\text{BSB}} = -t \sum_{\langle ij \rangle \ell} a_{i\sigma\ell}^\dagger b_{j\sigma\ell} - t_\perp \sum_i a_{i\sigma 2}^\dagger b_{i\sigma 1} + \text{h.c.}$$

$$+ U \sum_{i,\ell} \left(a_{i\uparrow\ell}^\dagger a_{i\uparrow\ell} a_{i\downarrow\ell}^\dagger a_{i\downarrow\ell} + b_{i\uparrow\ell}^\dagger b_{i\uparrow\ell} b_{i\downarrow\ell}^\dagger b_{i\downarrow\ell} \right), \quad (2)$$

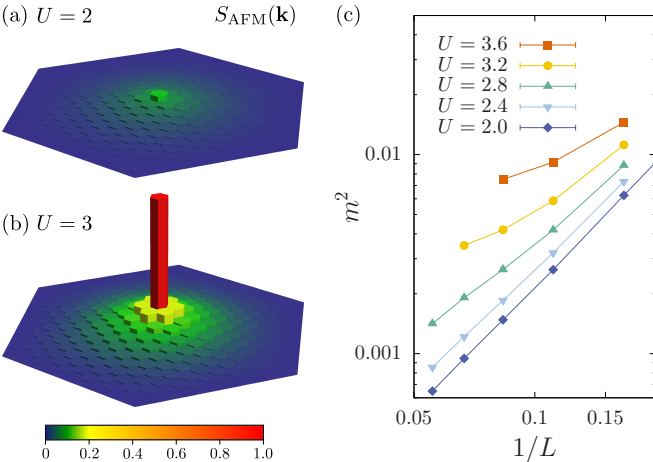


FIG. 2. Structure factor $S_{\text{AFM}}(\mathbf{k})$ and order parameter m^2 data for H_{BSB} with $t = t_\perp = 1$ (fixed throughout the paper). In (a) and (b) we show the structure factor in \mathbf{k} -space for an $L = 18$ lattice and its peak at Γ . Note the dramatic appearance of a Bragg peak structure as one changes from $U = 2$ to $U = 3$, indicative of a phase transition. (c) Finite size scaling of the order parameter $m^2 \equiv S_{\text{AFM}}(\Gamma)/L^2$, showing a finite m^2 for $U = 3.6$ and 3.2 , and then a dramatic suppression for smaller U .

where $\langle ij \rangle$ are bipartite nearest neighbors on the honeycomb layers. We choose $t = t_\perp = 1$, fixed throughout the manuscript (results for $t/t_\perp \neq 1$ are presented in the SM). This model has been studied previously where it was found that for $U/t > 3$ the model has Néel order. For $U/t < 3$ although no numerical evidence was found for the presence of Néel order in extrapolations of the order parameter, it was assumed based on functional RG calculations that the model was weakly Néel ordered [12], supporting the RG flow in Fig. 1(a) on the $\alpha = 0$ axis. Here we present clear numerical evidence that contrary to the previous conclusion, the system has a finite coupling phase transition at which magnetism appears.

To connect H_{BSB} with the long-wavelength description, Eq. (1), with only t, t_\perp hopping and $U = 0$, the system realizes Eq. (1) with $\alpha = 0$, a QBT arises described by the fixed point Q. Crucially, as noted earlier there is no symmetry that protects $\alpha = 0$. Indeed, trigonal hopping of the form $-t_3 \sum_{\langle ij \rangle \sigma} b_{i\sigma 2}^\dagger a_{j\sigma 1}$ preserves the symmetries of the bilayer and nonetheless has an α term, which makes the dispersion at low energies linear [5].

We emphasize that all our simulations are carried out with H_{BSB} itself and with no t_3 hopping. Thus H_{BSB} can be thought of as lying along the $\alpha = 0$ axis in Fig. 1(a,b).

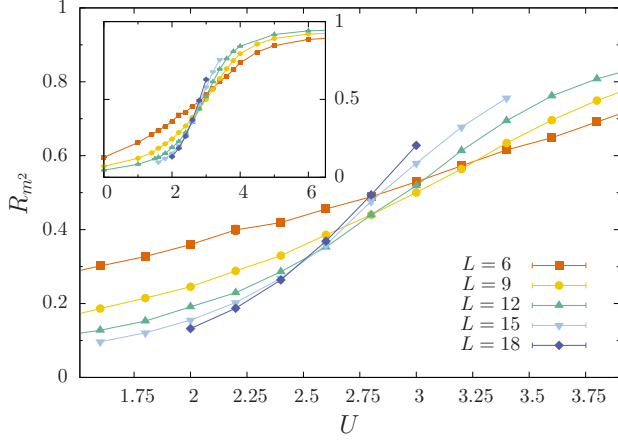


FIG. 3. Correlation ratio R_{m^2} , Eq. (3), close to the phase transition. The inset has a broad range of U showing how R_{m^2} reaches its asymptotes of 0 in the non-magnetic phase and 1 in the magnetic phase. At a continuous transition R_{m^2} is expected to be volume independent and cross at a universal value. The main panel show a zoom-in close to the critical point. The crossing point is at $U_c \approx 2.5$ with very small drifts on the largest systems sizes.

The two RG scenarios (a) and (b) make strikingly different prediction for the phase diagram of H_{BSB} . In scenario (a) H_{BSB} should flow to strong coupling even for arbitrarily small- U causing the system to Néel order for all U . In scenario (b), Néel order turns on at a finite order-one coupling through a relativistic quantum critical point. We now provide evidence using unbiased QMC simulations (the method used is reviewed in [16]) on H_{BSB} that as argued above RG scenario (b) is realized.

It is well known that the Hubbard model for $U/t \gg 1$ gives rise to the $S = 1/2$ Heisenberg model on the BSB, which has been convincingly demonstrated to have Néel order [12]. We now focus on the fate of the Néel order as U is weakened. In Fig. 2, we present data for the spin structure factor, $S_{\text{AFM}}(\mathbf{k}) \equiv \sum_{\mathbf{r}} e^{i\mathbf{k} \cdot \mathbf{r}} \langle \mathbf{S}(\mathbf{r}) \cdot \mathbf{S}(\mathbf{0}) \rangle$, where $\mathbf{S}(\mathbf{r}) = \sum_{\ell} (\mathbf{S}_{\ell A}(\mathbf{r}) - \mathbf{S}_{\ell B}(\mathbf{r}))$ is the unit cell anti-ferromagnetic order parameter, for various values of U . We expect a Néel ordered state to have a Bragg peak in the spin structure factor at the Γ point. As shown in Fig. 2(b) for $U = 3$, this is indeed the case. We find in Fig. 2(c) that $m^2 \equiv S_{\text{AFM}}(\Gamma)/L^2$ versus $1/L$ extrapolates to a finite value, indicating the divergence of the Bragg peak height as expected. As shown in (b), at $U = 2$ the peak gets rounded out. Consistent with this rounding out, we find in Fig. 2(c) that m^2 appears to extrapolate to zero in the thermodynamic limit for small U , indicative of a phase transition.

To study the long-distance ordering quantitatively rather than extrapolate m^2 (which is notoriously hard when m^2 is small [17]), we study the correlation ratio R_{m^2} of the structure factor at the ordering momentum (the Bragg peak) and the momentum closest to it \mathbf{b}/L

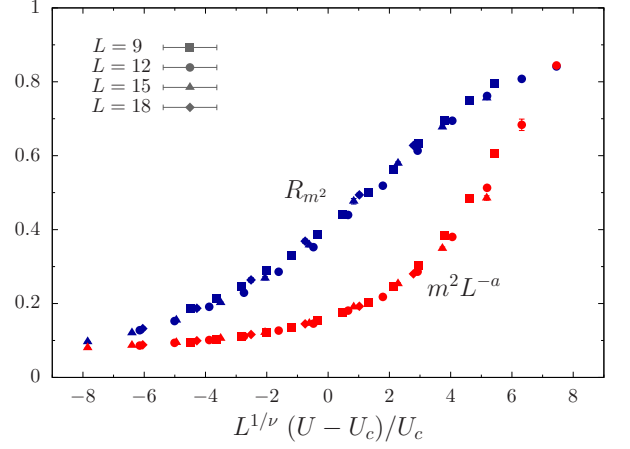


FIG. 4. Collapse of the magnetic data, m^2 and R_{m^2} close to the critical point. Parameters used for the collapse are $U_c = 2.6$, $\nu = 0.9$ and $a = 0.3$.

(\mathbf{b} is the shortest reciprocal lattice vector)

$$R_{m^2} = 1 - \frac{S_{\text{AFM}}(\Gamma + \mathbf{b}/L)}{S_{\text{AFM}}(\Gamma)}. \quad (3)$$

This quantity scales to 1 in an ordered phase and scales to 0 in a phase without a Bragg peak. At a quantum critical point R_{m^2} for different L cross at a universal value $R_{m^2}^*$. As has been emphasized in recent work this is a far more sensitive numerical test of the ordering than finite size extrapolations of the order parameter [18]. We note here that while R_{m^2} is able to sensitively diagnose whether a point in the phase diagram is ordered or not and hence locate the critical point, it cannot conveniently determine the value of the order parameter. In the inset of Fig. 3, our data for R_{m^2} clearly shows a transition from 0 to 1 that gets sharper as the system size increases. In the main panel, a zoom in of the data in the critical region shows a crossing. The crossing is at a value of $U_c \approx 2.5$ and does not drift significantly on all but the smallest lattices, providing strong evidence for a finite-coupling phase transition (see SM for more details).

Field theoretic arguments suggest that the transition between the Dirac phase and the Néel phase can be in the GN universality class. The key hallmarks of the GN class are: the gap in the Dirac fermions and the onset of magnetism take place at the same value of U and the emergence of Lorentz invariance or $z = 1$ critical scaling. To test for these features we study the collapse of the magnetic data (m^2 and R_{m^2}) and single particle gap Δ_{sp} , close to the transition. We have extracted Δ_{sp} from the decay of the imaginary time displaced Green function using standard methods [19, 20]. We collapse the magnetic data in Fig. 4, with the scaling forms $m^2 = L^a \mathcal{F}_{m^2} [L^{1/\nu}(U - U_c)/U_c]$ and $R_{m^2} = \mathcal{F}_{R_{m^2}} [L^{1/\nu}(U - U_c)/U_c]$, since the R_{m^2} has no scaling dimension. Corresponding windows for

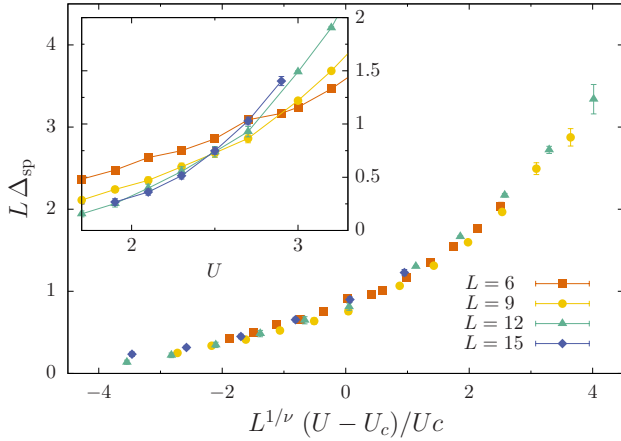


FIG. 5. The collapse of the single-particle gap $L\Delta_{\text{sp}}$ close to the phase transition with the same critical parameters as in Fig. 4 and $z = 1$. The inset shows the single-particle gap $L\Delta_{\text{sp}}$ as a function of U which exhibits a crossing at a coupling of $U_c \approx 2.5$, consistent with the expected scaling form with $z = 1$.

the parameters that give acceptable collapses are $U_c = 2.6(1)$, $\nu = 0.9(2)$ and $a = 0.3(1)$. For the gap, using standard finite-size scaling Ansatz, we expect $\Delta_{\text{sp}} = L^{-z} \mathcal{F}_\Delta [L^{1/\nu}(U - U_c)/U_c]$. We have verified that our data is consistent with this Ansatz with the values of the parameters extracted from the collapse for R_{m^2} and m^2 , and $z = 1$ in Fig. 5. Independently, we obtain acceptable collapses for Δ_{sp} for the ranges: $U_c = 2.5(2)$, $\nu = 1.0(2)$ and $z = 0.9(2)$. The inset in Fig. 5 shows our data for $L\Delta_{\text{sp}}$ versus U which should cross at the critical point if $z = 1$. We see a crossing in our data which is consistent with the crossings of R_{m^2} indicating the existence of a single transition at which both the magnetization turns on and the Dirac fermions get a mass. This is compelling evidence that the transition has $z = 1$, in contrast to the $z = 2$ scaling at the Q fixed point. Taken together, the identification of the quantum critical point with the GN class provides further evidence that H_{BSB} realizes the RG flow shown in Fig. 1(b).

We emphasize that our RG flow, Fig. 1(b) is only schematic: The point marked as D is used to describe collectively fixed points with a linear dispersion but which differ in the number and location of the Dirac cones. Even though we have provided strong evidence for a linear dispersion, we are unable to resolve from our QMC simulations which of these fixed points is realized in H_{BSB} . Our focus here has been on the phase diagram when $\alpha = 0$ in the microscopic model, i.e. the free problem has a QBT, such as in H_{BSB} . The evolution of the phase diagram with an explicit trigonal warping term in H_{BSB} and a more detailed study of the electronic structure will be presented separately.

To conclude, we have found that the quadratic band

touching in the Bernal stacked bilayer model is unstable to the formation of a linear dispersion when weak short-range interactions are added to it. Our results apply independently of the form of the short-range interactions [14], implying that generically models of bilayer graphene respond to interactions in much the same way as the single layer: symmetry breaking will only set in at an order-one coupling strength. In models with higher symmetry than the Bernal honeycomb bilayer the QBT can be symmetry protected [6, 21], then weak interactions are likely to flow to strong coupling and an RG flow as shown in Fig. 1(a) can be expected. It is of interest to simulate such models with unbiased QMC to verify this prediction and study the nature of the ordered phases. It is also interesting to revisit the fate of long-range Coulomb interactions on the quadratic band touching in light of our results.

We thank F. Assaad, C. L. Kane, C. Honerkamp, A. C. Potter, O. Vafeek, S. Wessel, A. Vishwanath and K. Yang for useful discussions. Financial support was received through NSF DMR-1056536. The numerical simulations reported in the manuscript were carried out on the NSF XSEDE allocation DMR150037.

-
- [1] A. H. Castro Neto, F. Guinea, N. M. R. Peres, K. S. Novoselov, and A. K. Geim, *Rev. Mod. Phys.* **81**, 109 (2009), URL <http://link.aps.org/doi/10.1103/RevModPhys.81.109>.
 - [2] I. F. Herbut, *Phys. Rev. Lett.* **97**, 146401 (2006), URL <http://link.aps.org/doi/10.1103/PhysRevLett.97.146401>.
 - [3] Z. Y. Meng, T. C. Lang, S. Wessel, F. F. Assaad, and A. Muramatsu, *Nature* **464**, 847 (2010), URL <http://dx.doi.org/10.1038/nature08942>.
 - [4] S. Sorella, Y. Otsuka, and S. Yunoki, *Sci. Rep.* **2**, 992 (2012), URL <http://www.nature.com/srep/2012/121218/srep00992/full/srep00992.html>.
 - [5] E. McCann and V. I. Fal'ko, *Phys. Rev. Lett.* **96**, 086805 (2006), URL <http://link.aps.org/doi/10.1103/PhysRevLett.96.086805>.
 - [6] K. Sun, H. Yao, E. Fradkin, and S. A. Kivelson, *Phys. Rev. Lett.* **103**, 046811 (2009), URL <http://link.aps.org/doi/10.1103/PhysRevLett.103.046811>.
 - [7] O. Vafeek and K. Yang, *Phys. Rev. B* **81**, 041401 (2010), URL <http://link.aps.org/doi/10.1103/PhysRevB.81.041401>.
 - [8] O. Vafeek, *Phys. Rev. B* **82**, 205106 (2010), URL <http://link.aps.org/doi/10.1103/PhysRevB.82.205106>.
 - [9] F. Zhang, H. Min, M. Polini, and A. H. MacDonald, *Phys. Rev. B* **81**, 041402 (2010), URL <http://link.aps.org/doi/10.1103/PhysRevB.81.041402>.
 - [10] R. Nandkishore and L. Levitov, *Phys. Rev. Lett.* **104**, 156803 (2010), URL <http://link.aps.org/doi/10.1103/PhysRevLett.104.156803>.
 - [11] Y. Lemonik, I. L. Aleiner, C. Toke, and V. I. Fal'ko, *Phys. Rev. B* **82**, 201408 (2010), URL <http://link.aps.org/doi/10.1103/PhysRevB.82.201408>.

- [12] T. C. Lang, Z. Y. Meng, M. M. Scherer, S. Uebelacker, F. F. Assaad, A. Muramatsu, C. Honerkamp, and S. Wessel, Phys. Rev. Lett. **109**, 126402 (2012), URL <http://link.aps.org/doi/10.1103/PhysRevLett.109.126402>.
- [13] V. Cvetkovic, R. E. Throckmorton, and O. Vafek, Phys. Rev. B **86**, 075467 (2012), URL <http://link.aps.org/doi/10.1103/PhysRevB.86.075467>.
- [14] We note that our RG argument assumes the model under study has particle-hole symmetry. This symmetry is present in all basic models of graphene systems including the H_{BSB} studied here, Eq. (2).
- [15] E. McCann and M. Koshino, Reports on Progress in Physics **76**, 056503 (2013), URL <http://stacks.iop.org/0034-4885/76/i=5/a=056503>.
- [16] F. F. Assaad and H. G. Evertz, Lect. Notes Phys. **739**, 277 (2008), URL http://dx.doi.org/10.1007/978-3-540-74686-7_10.
- [17] F. Parisen Toldin, M. Hohenadler, F. F. Assaad, and I. F. Herbut, Phys. Rev. B **91**, 165108 (2015), URL <http://link.aps.org/doi/10.1103/PhysRevB.91.165108>.
- [18] R. K. Kaul, Phys. Rev. Lett. **115**, 157202 (2015), URL <http://link.aps.org/doi/10.1103/PhysRevLett.115.157202>.
- [19] M. Feldbacher and F. F. Assaad, Phys. Rev. B **63**, 073105 (2001), URL <http://link.aps.org/doi/10.1103/PhysRevB.63.073105>.
- [20] T. C. Lang, Z. Y. Meng, A. Muramatsu, S. Wessel, and F. F. Assaad, Phys. Rev. Lett. **111**, 066401 (2013), URL <http://link.aps.org/doi/10.1103/PhysRevLett.111.066401>.
- [21] J. M. Murray and O. Vafek, Phys. Rev. B **89**, 201110 (2014), URL <http://link.aps.org/doi/10.1103/PhysRevB.89.201110>.

SUPPLEMENTAL MATERIALS

“Interaction induced Dirac fermions from quadratic band touching in bilayer graphene”

Sumiran Pujari,¹ Thomas C. Lang,² Ganpathy Murthy¹ and Ribhu K. Kaul¹

¹*Department of Physics & Astronomy, University of Kentucky, Lexington, KY-40506-0055*

²*Institute for Theoretical Physics, University of Innsbruck, 6020 Innsbruck, Austria*

RG ARGUMENTS

Generation of the linear kinetic term in perturbation theory

In this section we will show that even if one starts with a pure quadratic term at \mathbf{K} and \mathbf{K}' , second-order perturbation theory in the Hubbard interaction generates a linear term. First we collect a few pertinent facts. We will focus on momenta near one of the quadratic points, say \mathbf{K} for specificity. The bare kinetic term at $\mathbf{K} + \mathbf{k}$ looks like

$$\begin{pmatrix} 0 & -f^*(\mathbf{k})^2 \\ -f(\mathbf{k})^2 & 0 \end{pmatrix}. \quad (4)$$

For $|\mathbf{k}|$ small we can expand $f(\mathbf{k})$ as

$$f(\mathbf{k}) = -\frac{\sqrt{3}}{2}(k_x - ik_y) + \frac{1}{8}(k_x + ik_y)^2, \quad (5)$$

and hence we can approximate

$$[f(\mathbf{k})]^2 = C_0 k_-^2 + C_1 \mathbf{k}^2 k_+, \quad (6)$$

where $k_{\pm} = k_x \pm ik_y$. We will rescale momenta to make the number $C_0 = 1$ for future convenience.

In the Euclidean path integral the bare Green's function is

$$\mathcal{G}_{ij}(\omega, \mathbf{k}) = \frac{\delta_{ij}}{\omega^2 + |f(\mathbf{k})|^4} \begin{pmatrix} i\omega & -f^*(\mathbf{k})^2 \\ -f(\mathbf{k})^2 & i\omega \end{pmatrix}. \quad (7)$$

Here $i, j = 1, \dots, N$ label the flavours. We will confine ourselves to the momentum independent interactions which are marginal in the bare theory. As categorized by Vafeek (Ref. 8 of the main text), there are many classes of such interactions consistent with the symmetries. We will take the simplest one, the Hubbard interaction with N flavors, which comes with the unit matrix. Once again confining ourselves only to fields ψ_{ia} at the \mathbf{K} point, with $i = 1, \dots, N$ labelling the flavors and $a = 1, 2$ labelling the two-dimensional space of bands touching at the \mathbf{K} point we have the vertex

$$U \int d\mathbf{k}_1 d\mathbf{k}_2 d\mathbf{q} \sum_{i,j,a,b} : \bar{\psi}_{ia}(\mathbf{k}_1 - \mathbf{q}) \psi_{ia}(\mathbf{k}_1) \bar{\psi}_{jb}(\mathbf{k}_2 + \mathbf{q}) \psi_{jb}(\mathbf{k}_2) :. \quad (8)$$

The two diagrams contributing to the self-energy $\Sigma(\mathbf{k})$ to first order in U (1-loop) are

$$\Sigma^{(1)}(\mathbf{k}) = \text{Diagram 1} + \text{Diagram 2}.$$

It is easily seen that both diagrams give momentum-independent corrections, and hence cannot generate a linear term in \mathbf{k} near the \mathbf{K} point. The self-energy diagrams to second order in U are

$$\Sigma^{(2)}(\mathbf{k}) = \Sigma^{(1)}(\mathbf{k}) + N \text{Diagram 3} + \text{Diagram 4}.$$

It is clear that they have different dependences on N and hence cannot cancel for generic N . Therefore it is sufficient to examine the first one, setting the external frequency to zero, since we want the dependence on the spatial momentum. This diagram has the expression

$$\Sigma_{ij}(\mathbf{k}) = \frac{1}{(2\pi)^6} \int d\omega d\Omega d^2p d^2q \mathcal{G}_{ij}(-\Omega, \mathbf{k} - \mathbf{q}) \text{Tr} \left[\mathcal{G} \left(\omega + \frac{\Omega}{2}, \mathbf{p} + \frac{\mathbf{q}}{2} \right) \mathcal{G} \left(\omega - \frac{\Omega}{2}, \mathbf{p} - \frac{\mathbf{q}}{2} \right) \right]. \quad (9)$$

Of course the spatial momentum integrals must be cut off in some rotationally invariant way, by including factors such as $\exp(-\mathbf{k}^2/\Lambda^2)$, say. The crucial observation is that the result of carrying out the \mathbf{p} and ω integrals is a function which is rotationally invariant in \mathbf{q} . So

$$\frac{1}{(2\pi)^6} \int d\omega d^2p \text{Tr} \left[\mathcal{G} \left(\omega + \frac{\Omega}{2}, \mathbf{p} + \frac{\mathbf{q}}{2} \right) \mathcal{G} \left(\omega - \frac{\Omega}{2}, \mathbf{p} - \frac{\mathbf{q}}{2} \right) \right] = N F(\Omega, \mathbf{q}^2). \quad (10)$$

Now let us concentrate on the off-diagonal (in the a index) part of the self-energy, since that is where the linear term will manifest itself.

$$[\Sigma_{ij}(\mathbf{k})]_{12} = -\frac{NU^2}{(2\pi)^3} \int d\Omega d^2q F(\Omega, \mathbf{q}^2) \frac{(f^*(\mathbf{k} - \mathbf{q}))^2}{\Omega^2 + |f(\mathbf{p} - \mathbf{q})|^4}. \quad (11)$$

We focus on very small \mathbf{k} close to the \mathbf{K} point, expanding the integrand in powers of \mathbf{k} , keeping only up to first order in \mathbf{k} . Recalling that we have scaled momenta such that $C_0 = 1$ and up to higher orders we find the numerator to be

$$q_+^2 - 2k_+q_+ - C_1\mathbf{q}^2q_- + C_1(\mathbf{q}^2k_- + 2\mathbf{k} \cdot \mathbf{q}q_-), \quad (12)$$

while the denominator is

$$\Omega^2 + (\mathbf{q}^2)^2 - 4\mathbf{q}^2(\mathbf{k} \cdot \mathbf{q}) + C_1 [3\mathbf{q}^2(k_+q_+^2 + k_-q_-^2) + 2\mathbf{k} \cdot \mathbf{q}(q_+^3 + q_-^3)]. \quad (13)$$

We can now carry out the angular integral in d^2q . It is clear that no terms linear in \mathbf{k} survive the angular integral in the expansion of the denominator. However, a linear term does survive to first order in \mathbf{k} in the numerator. This is

$$- \frac{2NC_1U^2}{(2\pi)^3} k_- \int d\Omega d^2q F(\Omega, \mathbf{q}^2) \frac{\mathbf{q}^2}{\Omega^2 + (\mathbf{q}^2)^2}. \quad (14)$$

We have demonstrated that a term linear in \mathbf{k} is generically present in the two-loop correction to the self-energy.

Cartoon RG flow including the generation of the linear term at the QBT

We now examine what a cartoon of the RG flow might look like when we take the two-loop interaction generated linear term into account. Let us consider a single 4-point coupling g which is marginally relevant at the bare QBT fixed point with only quadratic terms in the kinetic energy. We will call the linear term in the kinetic energy α . The coupled RG equations will have the generic form

$$\frac{dg}{d\ell} = g^2, \quad \frac{d\alpha}{d\ell} = \alpha + Ag^2, \quad (15)$$

where A is some constant. The second equation follows from the fact that a linear term is relevant with scaling dimension 1 in the bare theory with a pure quadratic kinetic term. The initial conditions are $\alpha(0) = 0$; $g(0) = g_0 \ll 1$. Solving the first equation we find

$$g(\ell) = \frac{g_0}{1 - g_0\ell}, \quad (16)$$

so the scale at which $g(\ell_g) \approx 1$ is $\ell_g \approx \frac{1}{g_0}$. On the other hand we can solve the second equation with the initial condition as

$$\alpha(\ell) = Ae^\ell \int_0^\ell d\ell' g^2(\ell') e^{-\ell'}. \quad (17)$$

Clearly

$$\alpha(\ell) > Ag_0^2 e^\ell \int_0^\ell d\ell' e^{-\ell'} = Ag_0^2 (e^\ell - 1). \quad (18)$$

The scale at which $\alpha(\ell) \approx 1$ is therefore $\ell_\alpha \approx \log Cg_0^2$. For small enough g_0 it is clear that ℓ_α is parametrically smaller than ℓ_g , which means that the linear term becomes important far *earlier* in the RG flow than g as one flows to the infrared. We interpret this as a flow to a fixed point with a linear dispersion where interactions are well known to be irrelevant.

ADDITIONAL UNBIASED QMC DATA

Phase diagram in t_p - U plane

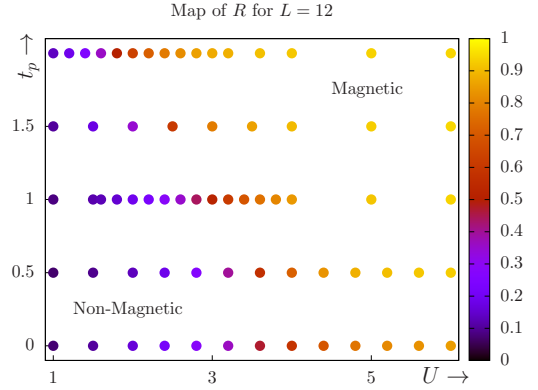


FIG. 6. A map of correlation ratio R_{m^2} vs t_p and U in units of $t = 1$, for $L = 12$.

In Fig. 6 we show a map of the correlation ratio R_{m^2} (defined in the main text) for $L = 12$ as t_p/t is tuned. For the case of $t_p/t = 1$, which was the focus in the main text, the critical value of U was found to be $U_c \approx 2.6$. Around this interaction strength the correlation ratio R is approximately $R_c \approx 0.4$ as can be seen in the above figure. By tracking where R_{m^2} crosses this approximate R_c we can see how the transition in the bilayer smoothly evolves in to that of the monolayer. Since we argue for Gross-Neveu criticality for the bilayer same as the monolayer in the main text, we may expect this smooth evolution of the critical point. Of course it is possible that there are Lifshitz like transitions where the number of Dirac nodes change inside the “non-magnetic” phase.

As $t_p/t \rightarrow \infty$, the quadratically touching bands become completely flat and we may expect that an infinitesimal value of Hubbard interaction strength immediately opens a gap. The evolution of U_c as t_p/t increases in in agreement with this expectation for the values of t_p/t studied.

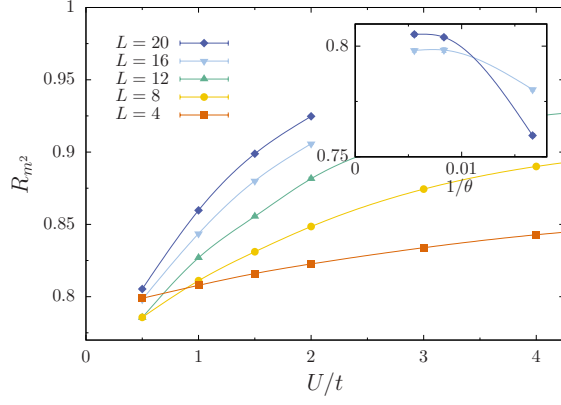


FIG. 7. Plot of R_{m^2} vs. U/t for half-filled Hubbard model on the square lattice. Note that contrary to the Honeycomb Bilayer case, the R value are greater than 0.75 for all values of U/t studied. Furthermore they are increasing with increasing system sizes and increasing projection lengths θ (see inset).

Correlation ratio for Square lattice Hubbard model at half-filling

In order to contrast the finite- U transition to the antiferromagnetic insulator on the honeycomb bilayer discussed in the main text, as evidenced by the correlation ratio R_{m^2} , we look at the corresponding quantity in the $SU(2)$ Hubbard model at half-filling on the square-lattice. Here we have a nested Fermi surface instead of Fermi points. As shown in Fig. 7, we see that there is antiferromagnetic ordering for all values of interaction U and system sizes L studied. This data is consistent with a $U \rightarrow 0^+$ instability. The results for R_{m^2} at the smallest value of $U = 0.5$ still increase with growing system sizes such that there is significant drift of the crossing points towards zero. This behavior is in contrast to the situation on the bilayer, where R_{m^2} clearly decreases as a function of system sizes for $U < 2.5$. Furthermore note the large values of R_{m^2} close to 1, far from the magnetically disordered limit of 0.

Comparison with Exact Diagonalization

In Table I, II, III we tabulate several observables computed using a ground state projection version of determinantal QMC with Exact Diagonalization (ED) for several observables. The system size is $L_x = 2$, $L_y = 1$ which corresponds to 8 sites. The two unit cells are indexed as $\mathbf{r}_1 = (0, 0)$ and $\mathbf{r}_2 = (1, 0)$. The 4 lattice sites per unit cell are further indexed by an integer μ ranging from 1 to 4. Parameters of the Hamiltonian were chosen to be $N = 2$ and $t = t_p = U = 1.0$. θ represents the length of ground-state projection $e^{-\theta H}$ applied on a trial state to reach the ground state. $d\tau$ represents the discretization of projection length and gives rise to Suzuki-Trotter

errors as seen in Table I, II, III.

Observable	ED	QMC	θ	$d\tau$
Total Energy	-14.7555...	-14.755(1)	40	0.05
		-14.755(1)	40	0.1
		-14.751(1)	40	0.2
		-14.755(1)	80	0.05
		-14.7553(6)	80	0.1
		-14.751(1)	80	0.2
Kinetic Energy	1.7648...	1.7664(5)	40	0.05
		1.7715(3)	40	0.1
		1.7895(3)	40	0.2
		1.7669(2)	80	0.05
		1.7714(2)	80	0.1
		1.7890(3)	80	0.2
Potential Energy	-16.5203...	-16.522(1)	40	0.05
		-16.527(1)	40	0.1
		-16.5403(5)	40	0.2
		-16.5214(5)	80	0.05
		-16.5267(5)	80	0.1
		-16.5402(5)	80	0.2

TABLE I. Comparison between QMC and ED data for Energy observables

Observable	ED	QMC	θ	$d\tau$
$\langle S_z(\mathbf{r}_1, 2) S_z(\mathbf{r}_1, 2) \rangle$	0.277468...	0.27729(2)	40	0.05
		0.2766(1)	40	0.1
		0.27427(1)	40	0.2
$\langle S_z(\mathbf{r}_1, 2) S_z(\mathbf{r}_2, 2) \rangle$	0.001907...	0.001908(1)	40	0.05
		0.001881(3)	40	0.1
		0.001843(2)	40	0.2
$\langle S_z(\mathbf{r}_1, 3) S_z(\mathbf{r}_1, 4) \rangle$	-0.250728...	-0.25046(2)	40	0.05
		-0.24961(2)	40	0.1
		-0.24628(2)	40	0.2
$\langle S_z(\mathbf{r}_1, 3) S_z(\mathbf{r}_2, 4) \rangle$	-0.003163...	-0.00316(1)	40	0.05
		-0.003141(4)	40	0.1
		-0.003089(4)	40	0.2

TABLE II. Comparison between QMC and ED data for (diagonal) Spin-spin correlations

A projection length of $\theta = 40$ is found to be sufficient. Trotter errors are present for the spin correlations and Green's function values, but for larger systems of interest (as shown in the next section) statistical errors dominate Trotter errors which is the regime we would like to sit at in determinantal QMC computations.

Observable	ED	QMC	θ	$d\tau$
$\langle c^\dagger(\mathbf{r}_1, 1)c(\mathbf{r}_1, 2) \rangle$	0.467109...	0.4671(1)	40	0.05
		0.4670(1)	40	0.1
		0.46632(4)	40	0.2
$\langle c^\dagger(\mathbf{r}_1, 1)c(\mathbf{r}_2, 2) \rangle$	0.023232...	0.02322(5)	40	0.05
		0.02315(4)	40	0.1
		0.02282(3)	40	0.2
$\langle c^\dagger(\mathbf{r}_1, 1)c(\mathbf{r}_1, 3) \rangle$	-6.29608...E-9	0.00003(3)	40	0.05
		0.00031(3)	40	0.1
		0.00255(2)	40	0.2
$\langle c^\dagger(\mathbf{r}_1, 1)c(\mathbf{r}_2, 3) \rangle$	2.83007...E-9	0.00004(3)	40	0.05
		0.00025(3)	40	0.1
		0.00206(2)	40	0.2

TABLE III. Comparison between QMC and ED data for (off-diagonal) single-particle Green's functions.

Projection and Discretization Errors

In Fig. 8, we show the projection length (θ) dependence of the two main quantities of interest, namely the dimensionless correlation ratio R (first two panels) and

the antiferromagnetic order parameter m^2 (last panel) as defined in the main text, for a representative value of Hubbard parameter ($U = 2.$) in the weak-coupling phase. In the strong coupling phase, projection to the ground states is even faster because of finite single particle gap due to presence of (Néel) order. For both the quantities, we see that statistical errors completely dominate Trotter errors, since for each value of θ the data points corresponding to the two values of $d\tau$ are *always* within QMC errorbars of each other. This is pragmatic from a QMC point of view when statistical errors dominate systematic errors for systems of interest to us.

For R we see a θ dependence (second panel of Fig. 8) which evens out for $\theta \geq 40$, and all the data points for a given system size L for $\theta = \{40, 50, 60\}$ are within QMC errorbars of each other. This shows that a projection length of $\theta = 40$ is sufficient for ground state values. For m^2 (third panel of Fig. 8), a similar conclusion holds. A minor thing of note that can be seen in first panel of Fig. 8 is that in comparison to the full range of $R \in [0, 1]$, the full θ dependence for a given system size $\lesssim 5\%$ which suggests that the scenario described in the main text will be applicable to finite temperatures as well.

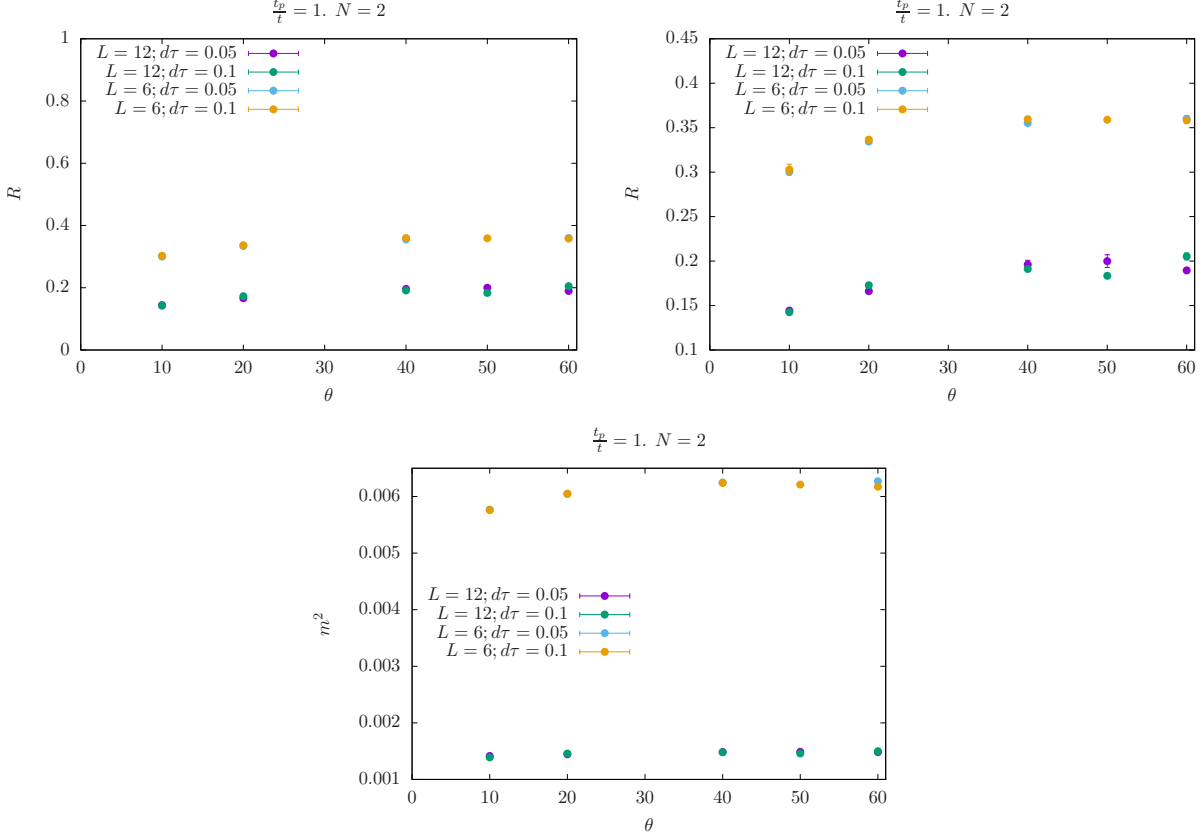


FIG. 8. Projection length (θ) dependence of correlation ratio R (first two panels) and AFM order parameter m^2 for a representative value of Hubbard parameter ($U = 2.$) in the weak-coupling phase.